The Journal of Molecular Diagnostics, Vol. 21, No. 2, March 2019

ELSEVIER

the Journal of Molecular Diagnostics
jmd.amjpathol.org

TECHNICAL ADVANCE

Combined Targeted Resequencing of Cytosine DNA Methylation and Mutations of DNA Repair Genes with Potential Use for Poly(ADP-Ribose) Polymerase 1 Inhibitor Sensitivity Testing

Christina Grimm,* Axel Fischer,† Angela M. Farrelly,‡ Roshni Kalachand,‡ Roberta Castiglione,§ Elena Wasserburger,* Michelle Hussong,*¶ Anne M. Schultheis,§ Janine Altmüller,‖ Holger Thiele,‖ H. Christian Reinhardt,¶**††‡‡ Kai Hauschulz,§§ Bryan T. Hennessy,‡ Ralf Herwig,¶¶ Matthias Lienhard,¶¶ Reinhard Buettner,§¶‖‖*** and Michal R. Schweiger*¶

From the Department of Translational Epigenetics and Tumor Genetics, the Institute of Pathology,§ the Center for Molecular Medicine Cologne,¶ the Cologne Center for Genomics,‖ the Clinic I for Internal Medicine,** the Center of Integrated Oncology,†† the Cologne Excellence Cluster on Cellular Stress Response in Aging-Associated Diseases,‡‡ and the Lung Cancer Group Cologne,‖‖ University Hospital Cologne, Cologne, Germany; icoder,† Potsdam, Germany; the Medical Oncology Group,‡ Department of Molecular Medicine, Royal College of Surgeons in Ireland, Dublin, Ireland; the Diagnostics and Genomics Group,§§ Agilent Technologies Sales and Services GmbH, Waldbronn, Germany; the Department of Computational Molecular Biology,¶¶ Max Planck Institute for Molecular Genetics, Berlin, Germany; and the Center for Integrative Oncology,*** University Hospital of Cologne and Bonn, Germany*

Accepted for publication October 16, 2018.

Address correspondence to Michal R. Schweiger, Ph.D., M.D., Translational Epigenetics and Tumor Genetics, University Hospital Cologne, Weyertal 115b, 50931 Köln, Germany. E-mail: mschweig@uni-koeln.de.

Current molecular tumor diagnostics encompass panel sequencing to detect mutations, copy number alterations, and rearrangements. However, tumor suppressor genes can also be inactivated by methylation within their promoter region. These epigenetic alterations are so far rarely assessed in the clinical setting. Therefore, we established the AllCap protocol facilitating the combined detection of mutations and DNA methylation at the coding and promoter regions of 342 DNA repair genes in one experiment. We demonstrate the use of the protocol by applying it to ovarian cancer cell lines with different responsiveness to poly(ADP-ribose) polymerase inhibition. *BRCA1*, *ATM*, *ATR*, and *EP300* mutations and methylation of the *BRCA1* promoter were detected as potential predictors for therapy response. The required amount of input DNA was optimized, and the application to formalin-fixed, paraffin-embedded tissue samples was verified to improve the clinical applicability. Thus, by adding DNA methylation values to panel resequencings, the AllCap assay will add another important level of information to clinical tests and will improve stratification of patients for systemic therapies. *(J Mol Diagn 2019, 21: 198—213; https://doi.org/10.1016/j.jmoldx.2018.10.007)*

New approaches in personalized medicine have revolutionized previous nonselective cancer therapies. Genetic or epigenetic markers are used to select optimal chemotherapies for individual patients.[1—3] One of the most exciting examples is the application of poly(ADP-ribose) polymerase (PARP) inhibitors to specifically treat platinum-sensitive, relapsed, breast cancer (BRCA) 1— or BRCA2-defective ovarian cancers. BRCA1 and BRCA2 are implicated in homologous

Supported by the Land of North Rhine-Westphalia; European Regional Development Fund EMODI grant EFR-0800397 (M.R.S.); the VolkswagenStiftung Lichtenberg program (H.C.R. and M.R.S.); the Center for Molecular Medicine Cologne (M.R.S., R.B., and H.C.R.); German Research Foundation grants KFO286 SCHW1605/1-1 (M.R.S.) and KFO-286-RP2 (H.C.R.); the German-Israeli Foundation for Research and Development grant I-65-412.20-2016 (H.C.R.); the German José Carreras Leukaemia Foundation grant R12/08 (H.C.R.); the Else Kröner-Fresenius Foundation grants EKFS-2014-A06, 2016_Kolleg.19 (H.C.R.); the Deutsche Krebshilfe grants 1117240 and 70113041 (H.C.R.); and the German Ministry of Education and Research grant e:Med 01ZX1303A (H.C.R.).

Disclosures: K.H. is employed by Agilent Technologies Sales & Services GmbH. H.C.R. received consulting and lecture fees from Abbvie, AstraZeneca, Vertex, and Merck. H.C.R. received research funding from Gilead Pharmaceuticals.

https://doi.org/10.1016/j.jmoldx.2018.10.007

recombination (HR)—mediated DNA double-strand break repair, whereas PARP1 plays a major role in base excision repair.[4,5] Targeting PARP in BRCA1/2-defective tumors results in failure of at least two DNA repair pathways with detrimental effects on the tumor cell.[4–6] Although PARP inhibitors (PARPi) are currently approved for *BRCA1*-mutant cancer, their therapeutic indication will likely extend to cancers displaying a BRCAness phenotype.[7] These tumors display a defective HR DNA repair in the absence of *BRCA1* or *BRCA2* mutations.[8] Furthermore, many clinical studies are investigating the use of PARPi in a wider spectrum of tumors (eg, prostate, breast, lung, and colon cancer).[9,10]

Defects in DNA repair mechanisms can be due to mutations or hypermethylation within promoter regions and subsequent down-regulation of the corresponding gene.[4,11–14] As far as genetic alterations are concerned, clinical studies investigating the effect of PARPi according to mutations in selected DNA repair genes are already ongoing (eg, clinical trials NCT03061188, NCT02286687, and NCT02987543). However, to broaden the analyses, and thereby improving the stratification of patients who will respond to PARPi, integrative analysis of DNA methylation and mutations in the same tumor sample is required. Such technologies covering both—epigenetics and genetics—for a set of genes are not yet available. Considering the growing number of targeted therapies and biomarkers predictive of therapy response, cost-effective assays capable of assessing the mutational and methylation status of multiple genes are needed.

In the clinical diagnostic setting, panel sequencing of single to hundreds of genes is well established and a few gene panels were already approved or cleared by the US Food and Drug administration: the Oncomine Dx Target Test by Thermo Fisher Scientific (Waltham, MA), analyzing 23 cancer-related genes; the FoundationOne CDx by Foundation Medicine (Cambridge, MA)[15]; and the MSK-Impact[16] (Integrated Mutation Profiling of Actionable Cancer Targets) by the Memorial Sloan-Kettering Cancer Center (New York, NY). The latter two are based on a hybridization capture assay and encompass 324 or 468 genes, respectively. In contrast, US Food and Drug administration–approved diagnostic tests based on DNA methylation are rare. So far, only two DNA methylation–based US Food and Drug administration–approved diagnostic tests for cancer exist: *SEPT9* traded as Epi proColon by Epigenomics AG (Berlin, Germany)[17,18] and Cologuard by Exact Sciences Corp. (Madison, WI), which probe multiple DNA methylation and genetic markers and a test for occult blood in feces. In addition to these approved tests, Epigenomics is developing a methylation-based test for lung cancer on methylation sites in the *SHOX2* and *PTGER4* genes, which already received a Conformité Européene—in vitro diagnostic (CE-IVD) mark in Europe. Several other clinically relevant DNA methylation alterations exist—some of which directly influence diagnostic and therapeutic decisions.[11,12,19] Hypermethylation of the *MLH1* promoter, for example, is used to discriminate hereditary and sporadic colorectal cancers, and methylation of the *MGMT* promoter indicates greater sensitivity to the alkylating agent temozolomide in glioblastoma multiforme.[2,3] Moreover, a recent *in silico* analysis identified 39 hypermethylated DNA damage repair genes in human cancers, which may represent novel therapeutic targets for DNA damage repair targeting therapies.[20] Approved clinical tests for these alterations do not exist, and methylation analyses are rarely undertaken in the clinical setting. This is partly due to the additional work required for investigating single loci and, on the other side, due to the intense costs for large-scale epigenetic analyses.[21,22]

Most techniques for the analysis of DNA methylation rely on bisulfite conversion of unmethylated cytosines to uracil, followed by high-throughput sequencing or single-locus analysis.[23] Whole genome approaches, such as whole genome bisulfite sequencing, theoretically cover all 28 million CpGs present in the human genome and are far too expensive for most studies. Medium throughput assays, such as the Methyl-Seq approach by Agilent Technologies (Waldbronn, Germany), the SeqCap Epi CpGiant Probes by Roche Sequencing (Pleasanton, CA), or the TrueSeq Methyl Capture EPIC kit by Illumina (San Diego, CA), cover large genomic regions of 84 Mb and 3.7 million CpGs, 80.5 Mb and 5.5 million CpGs, or 107 Mb and 3.3 million CpGs, respectively. The latest version of methylation arrays, the Infinium MethylationEPIC Bead Chip Kit (Illumina), interrogates 850,000 CpGs across the genome. Single loci are investigated by pyrosequencing technologies, which can perform methylation analyses on a large set of samples, but with only one position at a time. The establishment of these technologies surpasses the capability of most clinical diagnostic laboratories.

To overcome the technical limitations of only detecting genetic alterations, a protocol was developed, which combines methylation detection and mutational analyses of a panel of regions of interest by using a targeted hybrid selection and sequencing strategy. These regions cover 342 genes involved in DNA repair and investigated their mutational and DNA methylation status. As a proof of principle, nine ovarian cancer cell lines, sensitive or resistant to olaparib, were investigated. In addition, four PARPi-resistant cell line models were generated through a growth selection experiment in which clinical conditions of PARPi delivery were simulated. Finally, the applicability of the technology was shown for small DNA input amounts and for formalin-fixed, paraffin-embedded (FFPE) samples.

Materials and Methods

Ethics Approval and Written Consent

The study was approved by the ethics review board of the University Clinic of Cologne, under the reference number 13-091, and a written informed consent was obtained from the patient.

Cell Lines

The ovarian cancer cell lines A2780, CAOV3, ES2, FUOV1, OVCAR8, OVCA420, PEO1, SKOV3, and SNU251,[24] as well as the cell lines with acquired resistance (CAOV3-olaparib, CAOV3-talazoparib, OVCAR8-olaparib, and OVCAR8-talazoparib) were grown in RPMI 1640 medium (number 21875; Thermo Fisher Scientific, Waltham, MA) supplemented with 10% fetal bovine serum at 37°C and 5% CO_2. SNU251 was supplemented with 10 μg/mL insulin (C-52310; PromoCell GmbH, Heidelberg, Germany). Cell lines were short tandem repeats fingerprinted to confirm identity and regularly tested for *Mycoplasma* contamination using the MycoAlert PLUS detection kit (Lonza, Basel, Switzerland).

Cell lines with acquired resistance to a PARP inhibitor were developed after 5 months of continuous exposure of each parental cell line (CAOV3 or OVCAR8) to escalating doses of the PARP inhibitor (olaparib or talazoparib). A dose selection strategy was used for each cell line/drug combination to determine a starting dose that causes maximal cell kill, while allowing return to logarithmic cell growth. Selected doses corresponded to ≥IC80 values (inhibitory concentration at which 80% of the cells die) of the PARP inhibitor for that particular cell line, while remaining within the range of therapeutic drug levels observed in phase 1 pharmacokinetic data, to obtain clinically relevant resistant cell line models. For talazoparib, dose escalation beyond *in vivo* therapeutic levels was required to achieve stable resistant models. Parent cells were grown in parallel to the developing resistant cells. The established resistant cell lines were frozen at −80°C, then grown in drug-free media on defrosting, with resistance maintained on cytotoxicity assays assessed up to 15 weeks after defrost.

Cell Viability Assays

For each cell line, 1000 cells per well were seeded in a 96-well plate. After 24 hours, cells were treated with vehicle (dimethyl sulfoxide) and olaparib (Cayman Chemical Company, Ann Arbor, MI) at concentrations of 0.0, 0.30, 0.89, 2.67, 8.00, and 24.00 μmol/L (A2780, CAOV3, ES2, OVCAR8, SKOV3, SNU251, and PEO1) or at 0, 0.135, 0.625, 2.5, 10, and 40 μmol/L (FUOV1 and OVCA420) because for the latter a higher half maximal inhibitory concentration (IC_{50}) value was expected with regard to previously published experiments.[24,25] Growth was determined at 120 hours in triplicate by measurement of the ATP present, which signals the presence of metabolically active cells using the CellTiter-Glo Assay (Promega, Mannheim, Germany), according to the manufacturer's instructions. The luminescence was measured using a Tecan plate reader Infinite M1000PRO (Tecan, Maennendorf, Switzerland). The IC_{50} was determined from the regression of a plot of the logarithm of the concentration versus percentage inhibition at the time point of 120 hours using GraphPad Prism 7 (GraphPad Software, La Jolla, CA).

DNA Isolation

DNA from cell lines was isolated using the Qiamp DNA Mini kit (Qiagen, Hilden, Germany), according to the manufacturer's recommendations. DNA from FFPE material was isolated using the Qiamp DNA FFPE Tissue kit (Qiagen). DNA concentration was measured using the Qubit dsDNA BR fluorescence assay (Thermo Fisher Scientific) and a NanoDrop Spectrophotometer (Thermo Fisher Scientific) with similar results. DNA quality was assessed on a 1% agarose gel.

Capture Library

The custom design of the capture library was performed with the SureSelect DNA Advanced Design Wizard (Agilent Technologies, Waldbronn, Germany) on the GRCh37/hg19 genome build using the bait-boosting option balanced, which takes the GC content of the targeted regions into account by increasing the number of baits for GC-rich regions. The library consisted of 43,724 probes (7382 regions) encompassing 2.770 Mbp (design ID: 3080341) (Supplemental Table S1) with a recommended sequencing output of 554.186 Mbp. The coding and promoter regions of 342 genes implicated in the DNA damage response were included in the design (Supplemental Table S1). An intersection of the library regions with selected genomic features was performed using the University of California, Santa Cruz, Table Browser (*https://genome.ucsc.edu*).[26]

Methylation and Mutational Analysis

DNA was sheared to a size of 150 to 200 bp with a Bioruptor NGS (Diagenode, Seraing, Belgium) at 4°C for 6 × 10 cycles of 30 seconds on/off using high settings. Samples were vortex mixed and briefly centrifuged after every 10 cycles. DNA fragmentation was assessed with a High Sensitivity D1000 ScreenTape on a 2200 TapeStation (Agilent Technologies).

Library was prepared using the SureSelectXT Methyl reagent kit (number G9651A; Agilent Technologies) and Agencourt AMPure XP beads (Beckman Coulter, Krefeld, Germany), according to Agilent's recommendations (Agilent protocol: SureSelect^{XT} Methyl-Seq Target Enrichment System for Illumina Multiplexed Sequencing version D0; July 2015; G7530-90002; Santa Clara, CA) following the protocol for 3 μg input DNA. If 6 μg input DNA was used, two individual libraries were prepared, each with 3 μg of input DNA. The FFPE-DNA was repaired after shearing using the NEBNext FFPE DNA repair mix (New England Biolabs, Frankfurt am Main, Germany). Subsequently, libraries were prepared following the manufacturer's protocol for 1 μg input DNA.

Hybridization was performed using a custom-designed SureSelectXT 0.5 to 2.9 Mb library (number 5190-4816;

ELID: 3080341; Agilent Technologies) with the methyl-sequencing hybridization and enrichment reagents for 16 hours at 65°C, according to the manufacturer's protocol (Agilent protocol: SureSelect^{XT} Methyl-Seq Target Enrichment System for Illumina Multiplexed Sequencing version D0; July 2015; number G7530-90002). After hybridization, Dynabeads MyOne Streptavidin T1 (Thermo Fisher Scientific) were added to the hybridization mixture to capture the DNA/RNA-biotin hybrids and incubated according to the manufacturer's protocol. Subsequently, beads were washed. In the second washing step, beads were resuspended in 200 μL wash buffer and divided in two aliquots of 100 μL each. Each 100 μL aliquot was put on a magnetic separator, the wash buffer was completely removed, and the DNA was eluted. For the AllCap^{meth}, the beads were resuspended in 20 μL elution buffer and separated on a magnetic separator. The resulting eluted DNA was directly bisulfite converted using the EZ DNA Methylation Kit (Zymo Research, Freiburg, Germany) for 16 hours at 50°C, followed by a purification and two rounds of PCR amplification. A first round was performed with eight PCR cycles and a second round was performed with six PCR cycles using the SureSelectXT Methyl reagent kit.

For the target sequencing, the beads were resuspended in 30 μL H_2O and the bead-water mix was used in the first PCR amplification for eight cycles, followed by a second amplification for six cycles using the Herculase II Fusion DNA Polymerase (Agilent Technologies).

The amplified libraries were purified using Agencourt AMPure XP beads (Beckman Coulter). Concentration was determined using the Qubit dsDNA HS assay and a Qubit fluorometer (Thermo Fisher Scientific). The size and quality of the amplified libraries were tested using a High Sensitivity D1000 ScreenTape on a 4200 TapeStation (Agilent Technologies) as well as by quantification using the KAPA Library Quantification kit (Roche Diagnostics Deutschland GmbH, Mannheim, Germany) and the 7900HT Sequence Detection System (Applied Biosystems, Thermo Fisher Scientific), and sequencing was performed with an Illumina HiSeq4000 sequencer (Illumina) and a 75-bp paired end protocol. Venn diagrams were generated with Venny 2.1 [Oliveros, J.C. (2007-2015) Venny], an interactive tool for comparing lists with Venn diagrams (*http://bioinfogp.cnb.csic.es/tools/venny/index.html*, last accessed May 22, 2018).

Mutational Analysis

Paired-end sequencing was processed using the VARBANK version 1 pipeline of the Cologne Center for Genomics. In brief, reads were aligned to the human reference genome (GrCh37/hg19) using BWA-aln version 0.6.2, followed by duplicate marking (Picard version 1.64), base quality score recalibration, and local insertion/deletion realignment [both Genome Analysis Toolkit (GATK) version 1.6-11]. Mutations were called using the GATK best practice filter and an allele frequency of 10%. Information about allele frequencies or ClinVar annotations was obtained via the web interface of the Ensembl Variant Effect Predictor[27] using the Ensembl GRCh37, release 92. Variants with an allele frequency >0.01 in any population of the 1000 Genomes or the gnomAD Project or classified as benign or likely benign by ClinVar[28] were excluded from further analysis. The annotation was performed with Ensembl 68.

Methylation Analysis

Bisulfite-Sequencing Pipeline

Paired-end data were mapped against GrCh37/hg19 using bsmap v2.90 with default parameters, except the maximum allowed mismatches parameter (-v 0.1).[29] Samtools v1.4 was used to generate, sort, and index bam files and additionally generate mapping statistics, excluding secondary alignments (-F 256).[30] IntersectBed v2.20.1[31] was used to calculate the percentage of reads that intersect with designed target regions. In addition, exclusively on-target bam files were generated for the post mapping script methratio.py included in the bsmap v2.90 package to calculate base-wise and context-wise (CpG, CHG, CHH) methylation values with adapted parameters [-t 3 -u -p -z -g -x (CG|CHG|CHH)].[30] The methylation values calculated by the methratio.py script depict the ratios of reads with a methylated cytosine to the total number of reads covering one specific cytosine. Chromosomal positions in combination with coverage or methylation ratios were extracted to generate bedGraph formatted files to convert it afterward in BigWig format using bedGraphToBigWig of the University of California, Santa Cruz, utilities.[32] BigWig files were then loaded in the integrative genomics viewer v2.3.78 to visualize the results.[33,34] Metilene v0.2-7[35] was applied in de novo mode to call differential methylated regions between the following samples or sample sets: FFPE tumors versus FFPE normal; cell lines versus merged cell lines data of nine cell lines (A2780, CAOV3, ES2, FUOV1, OVCAR8_6μg_rep1, OVCA420, PEO1, SKOV3, and SNU251); OVCAR8_6μg_rep2, 3 μg, 1 μg against OVCAR8_6μg_rep1 and against merged cell line data and resistant CAOV3/OVCAR8 versus their corresponding parental cell line (CAOV3 or OVCAR8_6μg_rep1). Metilene filtering was set to $q < 0.05$ and a difference value of 0.3, except for the OVCAR8 comparisons, in which no difference value was applied. A cutoff of 0.3 was used because the interquartile range over all differentially methylated regions (DMRs) of all samples with q-value cutoff < 0.05 ranged between 0.19 and -0.15 (Supplemental Figure S1A). Because the hypermethylated regions are overrepresented in comparison to the hypomethylated regions, the absolute cutoff was used from the lower interquartile range: 0.15. Methylation values for a single cytosine can range between 0 and 1, but as differential methylation can be positive (hypermethylation) and negative (hypomethylation), ranging between -1 and 1, the absolute cutoff was doubled, resulting in an overall methylation difference cutoff for called DMRs of 0.3. At a q-value cutoff of

$q < 0.05$, 3409 DMRs were detected without a difference value cutoff; applying a difference value cutoff of 0.3, 536 DMRs were detected (Supplemental Figure S1B).

Visualization of base-wise methylation patterns of genes of interest was generated with a custom R script.

The methylation data were compared with the 450K methylation data from the Cancer Cell Line Encyclopedia project[25] (*https://www.ncbi.nlm.nih.gov/geo*; accession number GSE68379), available under the accession numbers: CAOV3/CAOV-3: GSM1669661; OVCAR8/OVCAR-8: GSM1670320; A2780: GSM1669581; ES2/ES-2: GSM1669769; PEO1: GSM1670347; FUOV1/FU-OV-1: GSM1669796; and SKOV3/SK-OV-3: GSM1670455. Data have been downloaded from the National Center for Biotechnology Information Gene Expression Omnibus repository and converted to β values in R with minfi v1.24.0.[36] Bland-Altman analyses were performed using GraphPad Prism 7.

Data Availability

Sequencing data of the cell lines are available at the National Center for Biotechnology Information (*https://www.ncbi.nlm.nih.gov/bioproject*; BioProject ID: PRJNA474810).

Results

Establishment of the AllCap Library for the Detection of DNA Methylation and Mutations in DNA Repair Pathway Genes

To set up a protocol for the detection of DNA methylation and mutation in a single assay, a hybrid-selection–based targeted technique, followed by post-capture bisulfite conversion,[37] was adapted. This technique is based on the hybridization of the targeted DNA to a biotin-labeled RNA strand and capturing the DNA-RNA hybrid by streptavidin. Sequencing libraries were first prepared from the DNA, and target capturing was performed. The captured DNAs were then divided into two parts, and one part was subjected to bisulfite conversion for methylation analysis and the other part to PCR amplification for mutation detection. During PCR amplification, indexes were included, such that both parts could be pooled and sequenced together (Figure 1A). In the following, we refer to the protocol as AllCap assay because all (mutations and methylation) can be captured, with DNA methylation analyses denoted as AllCap^{meth} and mutation analyses as AllCap^{mut}.

For the design of the capture library, exons as well as promoter regions and CpG island sequences were covered with probes. A total of 342 genes implicated in DNA repair were selected by searching the Reactome,[38] Kyoto Encyclopedia of Genes and Genomes,[39–41] and Repairtoire[42] databases and the Search Tool for the Retrieval of Interacting Genes (STRING)[43] database for BRCA1 interaction partners (Figure 1B and Supplemental Table S2). The designed library contains the promoter and the exons of the selected genes and encompasses 2.8 Mb with 72.808 CpGs (Supplemental Table S3). Of the targeted regions, 10% overlap with CpG islands, 42% with transcription factor binding sites, 58% at DNase I hypersensitive sites, and 63% with known genes (Figure 1C). Over all samples, a median of 52% and 55% of on-target reads was obtained for the AllCap^{mut} and AllCap^{meth} approaches, respectively, which is in the frame of routine target enrichment experiments with small library sizes.[44,45] The capture of coding and noncoding regions was similar (Supplemental Figure S2).

For the initial experiment, nine ovarian cancer cell lines (A2780, SNU251, OVCAR8, CAOV3, SKOV3, ES2, PEO1, FUOV1, and OVCA420) with known *BRCA1/2* mutation and *BRCA1* methylation status[24] and varying sensitivities to olaparib were used (Supplemental Figure S3 and Supplemental Table S4[24,46]). Libraries were prepared,

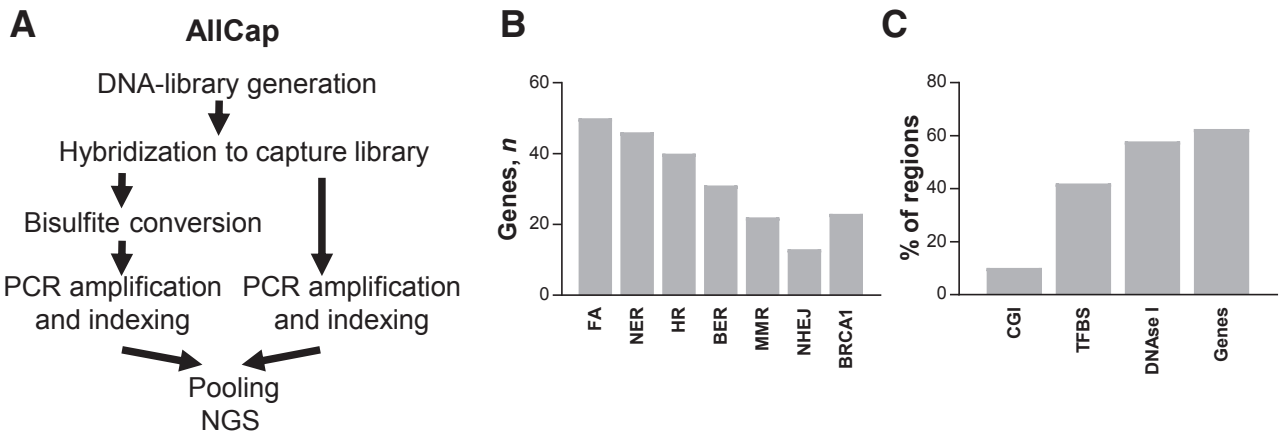

Figure 1 Experimental design. **A:** Experimental workflow illustrating the procedure of the AllCap protocol. **B** and **C:** Panel composition. **B:** The number of genes assigned to different Kyoto Encyclopedia of Genes and Genomes pathways or of the BRCA1 interaction partners denoted by STRING are given on the *y* axis. **C:** Percentage of the repair panel regions having any intersection with the indicated genomic features determined with the University of California, Santa Cruz (UCSC), Table Browser function. BER, base excision repair; BRCA1, BRCA1 interaction partner as denoted by STRING; CGI, CpG island; DNase I, DNase I hypersensitive clusters detected by ENCODE (DnaseClusteredV3); FA, Fanconi anemia; genes, UCSC known genes (hg19); HR homologous repair; MMR, mismatch repair; NER, nucleotide excision repair; NGS, next-generation sequencing; NHEJ, nonhomologous end joining; TFBS, transcription factor binding sites identified by the ENCODE project using chromatin immunoprecipitation followed by sequencing in different cell lines (TfbsClusteredV3).

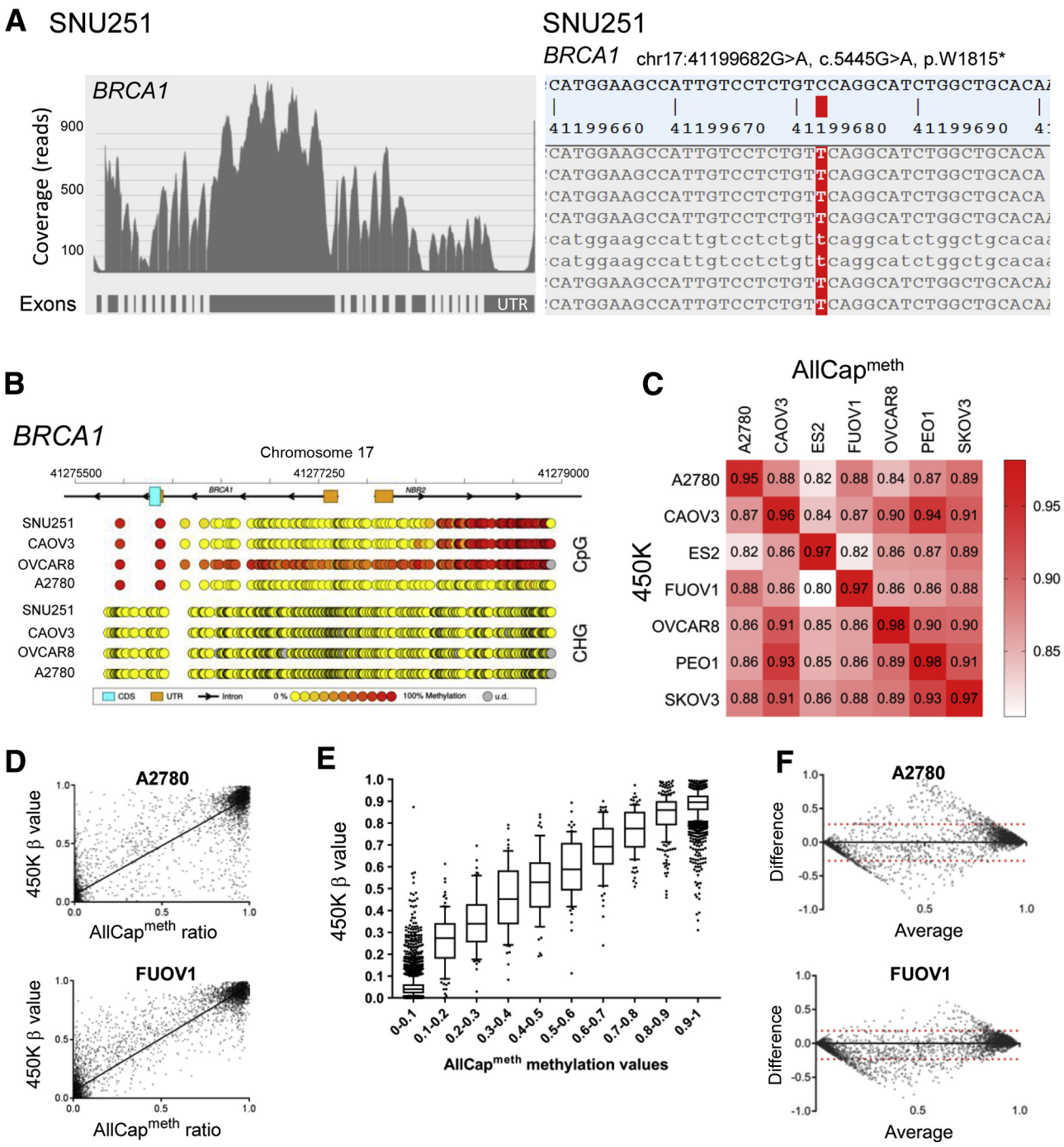

Figure 2 Data validation, correlation to publicly available data. **A:** Coverage plot for the *BRCA1* gene and visualization of the known homozygous *BRCA1* mutation (c.5445G>A, p.W1815*) in the SNU251 cell line. The mutated nucleotide is highlighted in red (T, because *BRCA1* is a reverse strand gene). Chromosomal positions refer to hg19. **B:** Visualization of the DNA methylation of the *BRCA1* promoter region. Each circle represents one CpG (**top four rows**) or one CHG (**bottom four rows**) as control, with yellow low and red high methylation values. OVCAR8 contains high promoter methylation of *BRCA1*.[24] **C:** Heatmap depicting Pearson's correlation between methylation values of the AllCap assay (AllCap^{meth}) and publicly available 450K methylation array data from the Cancer Cell Line Encyclopedia project (450K) calculated by GraphPad Prism 7. **D:** Examples of XY scatter plots visualizing the 450K array methylation β values on the *y* axis and the AllCap^{meth} methylation ratio values on the *x* axis. For the AllCap^{meth} data, a minimum coverage of 10 reads per CpG was required. A total of 6557 CpGs were measured by both assays. **E:** Comparison of the methylation values of 450K and AllCap^{meth}. Depicted are the 450K β methylation values on the *y* axis compared with the deciles of the AllCap^{meth} methylation values for OVCAR8 as an example. Given is the mean, the boxes represent the 25% to 75% range, and the whiskers represent the 10% to 90% range. **F:** Examples of Bland-Altman difference plots depicting the difference of the methylation values (AllCap^{meth} subtracted by 450K) on the *y* axis and the average of the AllCap^{meth} and the 450K methylation values on the *x* axis. **Dotted lines** depict the 95% CI (limits of agreement). CDS, coding sequence; chr17, chromosome 17; u.d., undetermined; UTR, untranslated region.

hybridized, and divided into two halfs, and from one part a bisulfite conversion was performed. For the amplification of bisulfite, converted DNA reagents from Agilent Technologies, which were optimized for bisulfite converted material, were used.

Both parts, the bisulfite-converted and the targeted one, were PCR amplified. During the second PCR amplification, indexes were added. Subsequently, libraries were pooled and sequenced with approximately 20 million reads output, corresponding to 1500 Mb, resulting in a mean coverage of approximately 230× for each, the targeted and the methylation sequencing (Supplemental Table S5). Of the 72,808 CpGs present in the bait library, 84 were not covered by any sample in the methylation sequencing (Supplemental Tables S3 and S6 and Supplemental Appendix S1). Because in mammals the predominant site of methylation occurs at CpG sites, and cytosines in a CHH or CHG context (where H = A,T, or C) remain mostly unmethylated, the bisulfite conversion rate was calculated from the CHH or CHG sites and a mean conversion rate of 99.2% was obtained for the nine cell lines (Supplemental Table S5). With this protocol, the reported homozygous *BRCA1* c.5564G>A, p.W1815* mutation was detected in the SNU251 cell line (Figure 2A and Supplemental Table S7[47–49]) and the hypermethylation of the *BRCA1* promoter was detected in the OVCAR8 cells[24] (Figure 2B and Supplemental Table S8). The obtained methylation values were then compared with the 450K data generated by the Cancer Cell Line Encyclopedia project.[25] For the analysis, 6557 CpG sites were assessed by both assays and had a coverage of at least 10 reads in our assay. Pearson's correlation for corresponding cell lines ranged between 0.925 and 0.953 (Figure 2C), and the X-Y scatter plots revealed a linear distribution (Figure 2D and Supplemental Figure S4A). However, in the low methylation range, the 450K array data report slightly higher values compared with the AllCap^{meth} values, whereas in the high methylation range, the 450K array data reported slightly reduced methylation values. This is also seen when comparing the 450K methylation values with the deciles of the AllCap^{meth} methylation values (Figure 2E). This peculiarity of the 450K array was already recognized in a study comparing several methylation assays.[23] To further compare the two methods, Bland-Altman analyses were performed (Figure 2F and Supplemental Figure S4B), which is commonly used to measure the difference between two methods. Comparing AllCap^{meth} with the 450K data using Bland-Altman revealed a median range for the limit of agreement of −0.23 to 0.19 at a 95% CI and a median bias of −0.01 over all seven comparisons. Moreover, the root mean square error for all seven array/AllCap^{meth} comparisons ranged between 0.095 and 0.139, indicating a good concordance of the two methods. These results revealed that the simultaneous detection of mutations and DNA methylation with one capture library is feasible and generates biologically relevant data for assessing PARPi sensitivity.

Mutations and Methylation Alterations in Ovarian Cell Lines Discovered with the AllCap Assay

In total, mutations were detected in 107 genes and the number of mutated genes per cell line ranged from 3 to 36 in the cell lines CAOV3 and A2780, respectively (Figure 3 and Supplemental Table S7). Both cell lines are sensitive to olaparib.

The most commonly mutated gene was *TP53*, which was observed in eight of the nine cell lines. The occurrence of mutations present in the olaparib-sensitive, but not in the resistant, cell lines was evaluated. Ataxia telangiectasia and rad3-related protein (*ATR*) and ataxia telangiectasia mutated (*ATM*) mutations were present in sensitive cell lines (CAOV3, SKOV3, and OVCAR8), which is in line with previously published work.[50–54] One *BRCA1* mutation (c.5564G>A, p.W1815*) was detected in SNU251, which in our analysis showed a medium sensitivity to olaparib with an IC_{50} value of 9.9 μmol/L after 5 days of treatment. However, this is probably due to a reduced doubling time of the SNU251 cells, and after 2 weeks of treatment, an IC_{50} of 2 μmol/L was measured.[24] In the more resistant PEO1 cell line, a deleterious homozygous *BRCA2* mutation (c.4965C>G, p.Y1655*) and a back mutation that reverses the acquired stop mutation [c.4964A>T, p.Y1655F, allele frequency (AF) = 0.35] as resistance mechanism were observed, as described previously.[24] Interestingly, mutations were detected in *EP300* solely in sensitive cell lines (A2780, SKOV3, and OVCAR8). *EP300* encodes the E1A binding protein P300, which acetylates histones and PARP1,[55] and PARP1 is activated on acetylation.[56] In addition, interaction of CREB binding protein (CREBBP)/EP300 with PARP1 promotes NF-κB activation,[57] and recently, olaparib was shown to up-regulate death receptors by NF-κB activation.[58] Moreover, PARP1 was described to recruit EP300 to a subset of promoters.[59]

Thus, besides known mutations in *BRCA1*, these data support a role of *ATM* and *ATR* mutations in mediating olaparib sensitivity[60] and point to *EP300* as a potential candidate for enhancing olaparib sensitivity.

DMRs were calculated by comparing the individual cell lines to the average methylation value of all nine cell lines, identifying 28 to 54 DMRs per cell line at a significance threshold of $q < 0.05$ (Supplemental Table S9). *BRCA1* and *MGMT* promoter DNA methylation were detected in the OVCAR8 cell line (Supplemental Table S8), which is sensitive to olaparib, with an IC_{50} of 4.8 μmol/L in our analysis.

Reproducibility of the Protocol and Reduction of the DNA Input Amount

Next, the reproducibility of the assay was tested using different DNA amounts. Therefore, replicates were performed with 6, 3, and 1 μg of input DNA from the ovary cancer cell line OVCAR8, and approximately 20 million reads per sample were generated. In comparison to conventional hybrid-capture

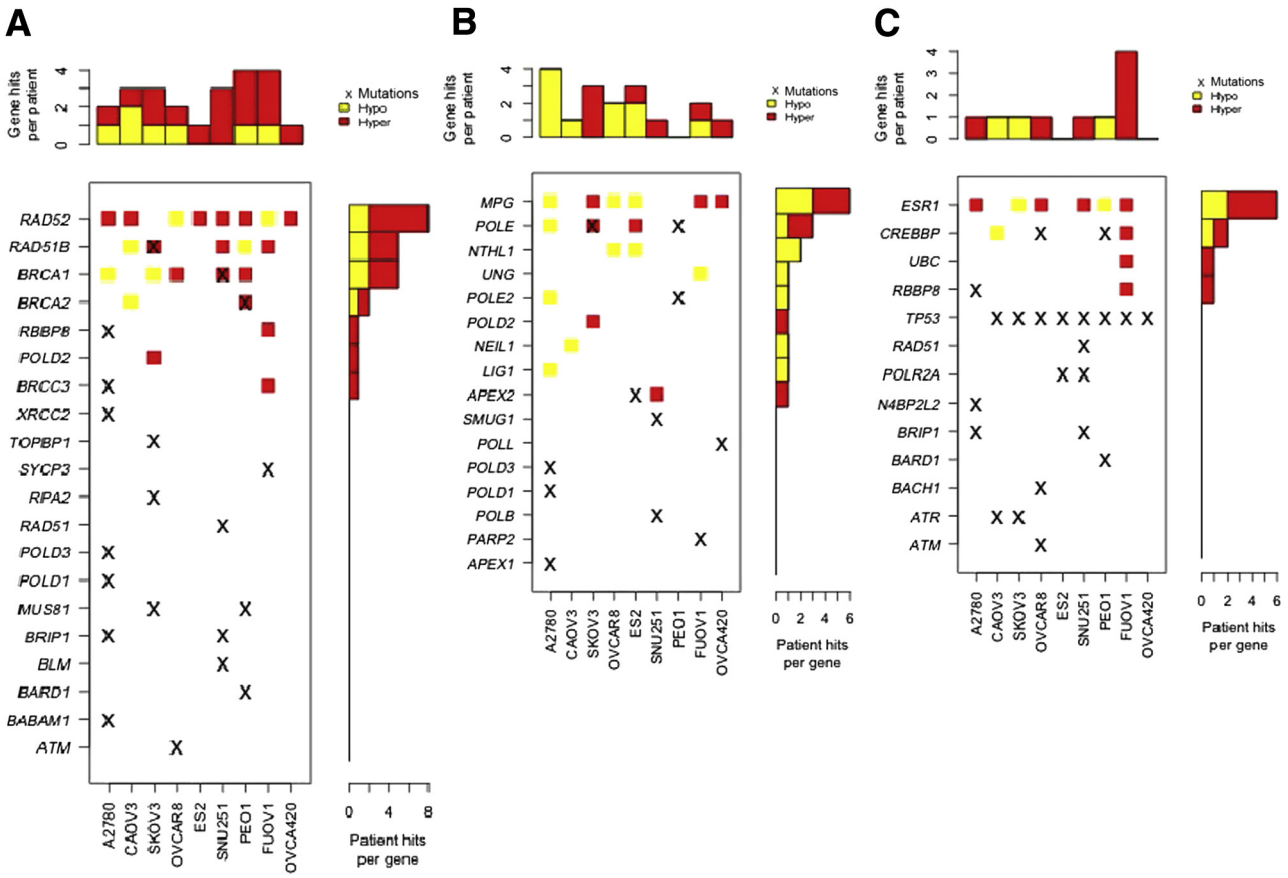

Figure 3 Mutations and differential methylation in homologous recombination genes (**A**), base excision repair genes (**B**), and BRCA1 interaction partners (**C**) detected in nine cell lines sorted according to their olaparib sensitivity (sensitive left, resistant right). Methylation alterations refer to observed alterations in the gene and/or the promoter regions. Red depicts hypermethylation; yellow, hypomethylation; crosses, mutations. Hyper; hypermethylation; Hypo, hypomethylation; SNP, single-nucleotide polymorphism alteration.

assays used for the initial experiments, rather high DNA input amounts were used to account for a low yield after bisulfite conversion. For the targeted sequencing, a slight reduction in unique reads was observed for 1 μg of input DNA (64% versus 71% to 80%) (Supplemental Table S5), indicating an increase in duplicate reads. For the AllCap^{meth}, the fraction of mapped reads and on-target reads was comparable between the different DNA input amounts (56% to 59%) and the calculated bisulfite conversion efficiency exceeded 99% for all four replicates (Supplemental Table S5).

The on-target coverage of the four replicates for the targeted sequencing and the AllCap^{meth} samples was evaluated. A marginal decrease in the coverage of the AllCap^{meth} samples was observed, which is most likely because of the reduced complexity of the bisulfite-treated samples, whereas the individual replicates did not show any obvious difference in target coverage (Figure 4A). Regarding mutation detection (AllCap^{mut}), in all four replicates, the identical protein-altering mutations were detected with similar allele frequencies, revealing reproducible mutation detection with DNA input amounts of 1 to 6 μg (Figure 4B and Supplemental Table S10[47–49]).

Subsequently, the global correlation of the methylation values was assessed by one-to-one comparisons of the different replicates. The Pearson's correlation coefficient of the replicates exceeds 0.995, whereas the correlation to an unrelated ovary cell line, A2780, was < 0.89, indicating an increased overall concordance between the replicates from 1 to 6 μg DNA input (Figure 4C). Next, the variation was assessed in local methylation levels by calculating the number of DMRs detected in one-to-one comparisons ($q < 0.05$). No DMRs were detected when comparing 6 with 3 μg, and one DMR was detected when comparing 6 with 1 μg of input DNA at a low methylation difference of 0.13 (Figure 4D). These results indicate reliable detection of methylation using 3 μg of input DNA. For 1 μg of input DNA, more detailed analyses (eg, with inclusion of absolute methylation values) are needed.

To verify the reproducibility of DMR detection, each of the four replicates was compared with the average methylation values generated from nine different cell lines ($q < 0.05$) (Supplemental Table S8). Adjacent DMRs that were <500 bp apart were merged. After merging, 31 to 35

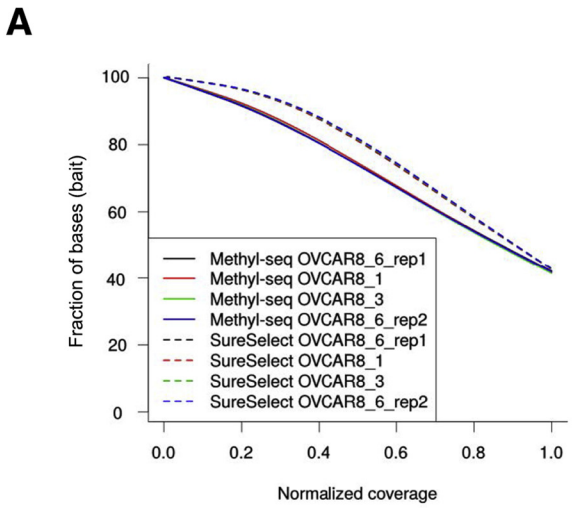
A
Fraction of bases (bait)
Normalized coverage
Methyl-seq OVCAR8_6_rep1
Methyl-seq OVCAR8_1
Methyl-seq OVCAR8_3
Methyl-seq OVCAR8_6_rep2
SureSelect OVCAR8_6_rep1
SureSelect OVCAR8_1
SureSelect OVCAR8_3
SureSelect OVCAR8_6_rep2

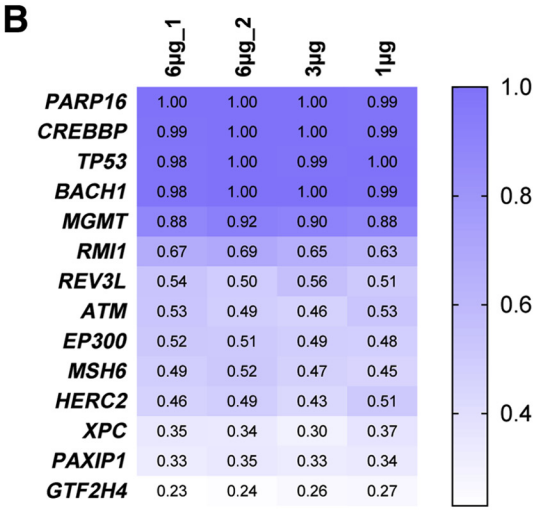
B
6µg_1 6µg_2 3µg 1µg
PARP16 1.00 1.00 1.00 0.99
CREBBP 0.99 1.00 1.00 0.99
TP53 0.98 1.00 0.99 1.00
BACH1 0.98 1.00 1.00 0.99
MGMT 0.88 0.92 0.90 0.88
RMI1 0.67 0.69 0.65 0.63
REV3L 0.54 0.50 0.56 0.51
ATM 0.53 0.49 0.46 0.53
EP300 0.52 0.51 0.49 0.48
MSH6 0.49 0.52 0.47 0.45
HERC2 0.46 0.49 0.43 0.51
XPC 0.35 0.34 0.30 0.37
PAXIP1 0.33 0.35 0.33 0.34
GTF2H4 0.23 0.24 0.26 0.27

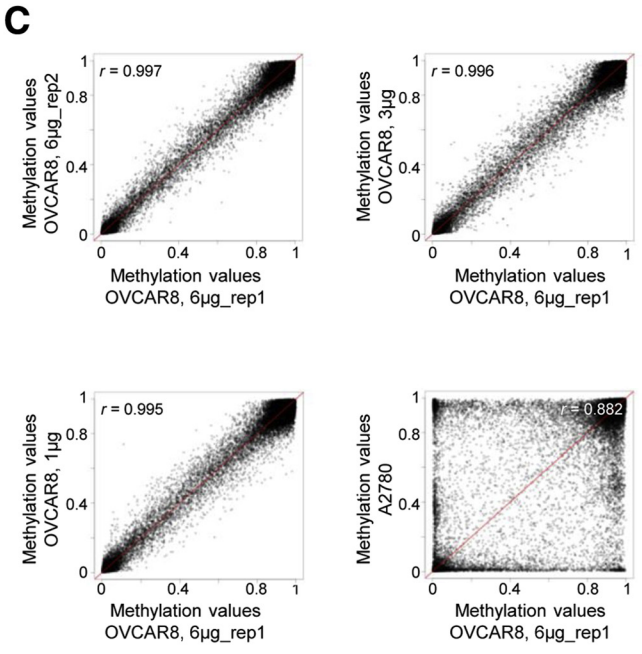
C
r = 0.997
r = 0.996
r = 0.995
r = 0.882
Methylation values OVCAR8, 6µg_rep2
Methylation values OVCAR8, 3µg
Methylation values OVCAR8, 1µg
Methylation values A2780
Methylation values OVCAR8, 6µg_rep1

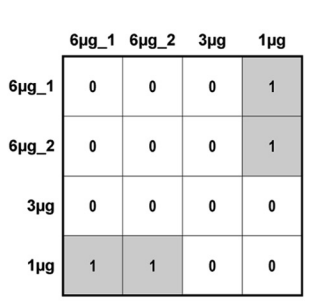
D
6µg_1 6µg_2 3µg 1µg
6µg_1 0 0 0 1
6µg_2 0 0 0 1
3µg 0 0 0 0
1µg 1 1 0 0

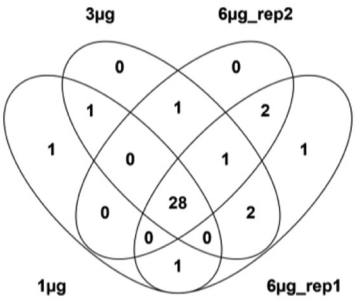
E
3µg
6µg_rep2
1µg
6µg_rep1
0 0 1 1 2 1 0 1 0 28 2 0 0 1

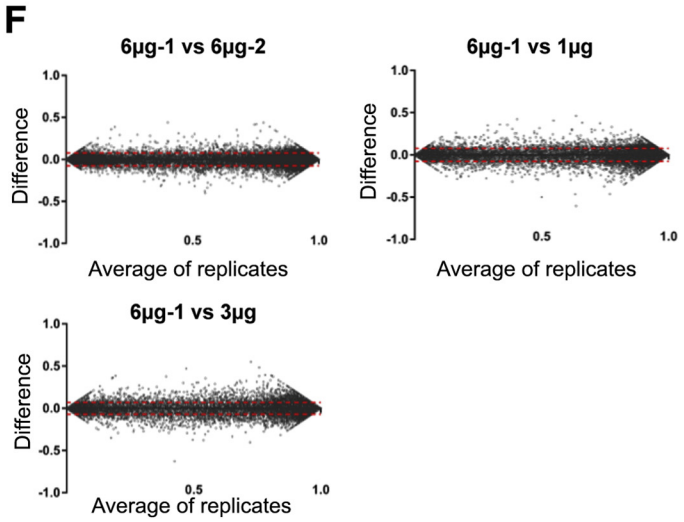
F
6µg-1 vs 6µg-2
6µg-1 vs 1µg
6µg-1 vs 3µg
Difference
Average of replicates

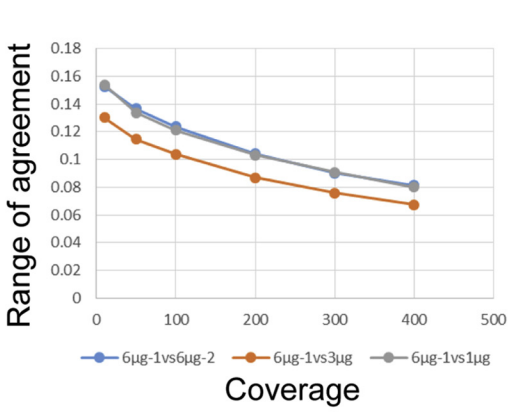
G
Range of agreement
Coverage
6µg-1vs6µg-2
6µg-1vs3µg
6µg-1vs1µg

DMRs were obtained per replicate, of which 28 were detected in all four replicates (Figure 4E). Finally, Bland-Altman analyses were performed and a limit of agreement between our replicates was found at 10× coverage between −0.08 and 0.08 (Figure 4F). With an increase in coverage, the range of the mean limit of agreement decreases to −0.04 to 0.04 at 400× coverage (Figure 4G), indicating a good reproducibility of the AllCap assay.

Assessment of the Suitability of AllCap for FFPE Material

To test whether archived FFPE material from clinical tissue specimens can be used for the AllCap assay, two tumor and one matched normal FFPE specimen from a T-cell lymphoma patient were used. The tumor contains a known somatic *ATM* c.6326G>A, p.W2109* mutation. For the two tumor samples, 0.9 and 0.25 μg DNA were used, respectively, and for the normal sample, 1.2 μg DNA was used. For targeted sequencing, approximately 20 × 10^6 reads were generated per sample and thereof approximately 50% were uniquely mapped for the two samples with 0.9 and 1.2 μg of input DNA. When 0.25 μg of input DNA was used, only 23% of reads were uniquely mapped, revealing a high number of off-target reads or duplicate reads. Nevertheless, analyzing the mutations, the known tumor-specific *ATM* mutation p.W2109* was reliably detected in both tumor specimens with similar allele frequencies and coverage rates. Three additional tumor-specific nonsynonymous mutations were detected in both tumor samples (Supplemental Table S11[47–49]), indicating that reduced DNA input amount still allows the correct identification of mutations.

A similar result was observed with the AllCap^{meth} protocol, in which 43% and 47% of on-target reads were obtained for the two samples with >0.9 μg of input DNA and 28% for the sample with 0.25 μg input DNA. The calculated bisulfite conversion efficiency was 92.9% for the 0.25 μg DNA input sample compared with 98% and 98.4% for the two other FFPE samples (Supplemental Table S5). This result indicates that a low DNA input amount results in a reduced bisulfite conversion rate as well as in an increase of duplicate and off-target reads. However, for a coverage of 74×, the fraction of baits covered by the three FFPE samples was comparable between the different samples (Figure 5A).

Comparing the global DNA methylation of tumor 1 (0.9 μg input) and tumor 2 (0.25 μg input) with normal reveals Pearson's correlation coefficients of 0.97 and 0.96, respectively, and between the two tumors of 0.98, indicating a high degree of concordance between the three samples. A high concordance of global methylation, even between tumor and normal, is conceivable because the specimens were derived from the same individual and, especially, because our targeted panel is small and only focal DNA methylation alterations are expected. However, regardless of the high correlation values, the scatter plot reveals a diversification of the methylation values in the tumor versus normal comparisons in contrast to the comparisons between the tumors (Figure 5B).

The identification of focal methylation alterations revealed 23 DMRs (17 hypermethylated and 6 hypomethylated) for tumor 1 versus normal and 31 DMRs (26 hypermethylated and 5 hypomethylated) for tumor 2 versus normal, of which 16 DMRs in 15 genes were detected in both tumor specimens (11 hypermethylated and 4 hypomethylated) (Supplemental Table S12). Examples displaying the *EYA4* and *MGMT* promoter are shown in Figure 5C. *EYA4* encodes the eyes absent homolog 4, a transcriptional coactivator and phosphatase and is frequently methylated in tumors.[61] *MGMT* encodes a O(6)-methylguanine-DNA methyltransferase, which is responsible for the repair of methylated O(6)guanine adducts. A hypermethylation of the *MGMT* promoter can result in gene silencing and a failure to repair the mutagenic O(6)guanine adducts. It is a favorable prognostic marker for the response to radiation or chemotherapy (eg, temozolomide) in glioblastoma.[12–14] In the tumor 2 specimen, a DMR was called in the *MGMT* promoter; however, this DMR did not reach the significance level of $q < 0.05$, probably because of the lower bisulfite conversion rate (92%) of this sample (Figure 5D and Supplemental Tables S5 and S12).

Mutations and DNA Hypermethylation in Cell Lines with Acquired Resistance

To identify resistance mechanisms of PARP inhibition, two cell line pairs with acquired resistance to the PARPi olaparib

Figure 4 Evaluation of the reproducibility and reduction of input amount for the AllCap assay. **A:** Normalized coverage plot of the technical replicates with different input amounts. The fraction of baits (nucleotides) is given on the *y* axis, and the normalized coverage is given on the *x* axis. **B:** Mutation detection in the replicates of OVCAR8. Given are the detected allele frequencies of protein altering mutations. **C:** Pearson's correlation of the methylation levels of the technical replicates and different input amounts and for comparison of an unrelated cell line (A2780; **bottom right panel**). As reference, one of the 6-μg input amount sample was used and compared with the second 6-μg sample (**top left panel**), the 3-μg input sample (**top right panel**), and the 1-μg input sample (**bottom left panel**). Only CpGs covered in all samples by ≥10 reads were used for the correlation calculation. Methylation levels of 0 and 1 were excluded from the calculation. **D:** Differentially methylated regions (DMRs) detected in the replicates of OVCAR8 cells. Pairwise comparisons were calculated by metilene, filtered for significance ($q < 0.05$). The number of detected DMRs is given. **E:** Intersection of DMRs that were called by pairwise comparisons of the individual OVCAR8 replicates with the average methylation value of nine different cell lines is depicted as a Venn diagram generated by Venny 2.1. **F:** Bland-Altman difference plots depicting a high concordance of the replicates. The difference of the two replicates is depicted on the *y* axis, and the average of the two replicates is depicted on the *x* axis. **Dotted lines** depict the 95% CI (limits of agreement). **G:** Given is the range of agreement on the *y* axis and the coverage cutoff on the *x* axis, revealing a decrease in variability at higher coverages. Seq, sequencing.

or talazoparib were analyzed (Supplemental Table S4 and Figure 6). These cell lines were generated by continuous growth of sensitive parental cell lines (CAOV3 or OVCAR8) in the presence of either drug over 5 months.

As denoted earlier, parental CAOV3 cells carry homozygous mutations in *TP53* (c.406C<T, p.Q136*) and *USP45* (c.1196A>G, p.N399S), and it is the cell line with the least mutations in our DNA repair gene panel. Interestingly, the parental CAOV3 cells carry a mutation in *ATR* (c.569A>T, p.Q190L) with an allele frequency of 0.19. This *ATR* mutation was not detected in the olaparib-resistant cells, but is present in the talazoparib-resistant cells with an allele frequency of 0.46 (Supplemental Table S13[47–49]). Because an *ATR* mutation was not detected in the Cancer Cell Line Encyclopedia data set[25] and has a rather low allele frequency of 0.19 in the parental CAOV3 cells, it is conceivable that this mutation is an example of clonal evolution in the CAOV3 cell line. Interestingly, inhibition of ATR can overcome PARPi resistance[51,52]; therefore, an initial *ATR* mutation with a small allelic fraction may be deleted in the olaparib-treated cells. Moreover, PARPi treatment increased phosphorylated ATR and a combination treatment of PARP and ATR inhibitors synergistically decreased survival in a cell line model.[50] However, this mutation was stable in the talazoparib-resistant cells, indicating alternative mechanisms of PARPi resistance in this cell line.

In regard to the DMRs in CAOV3 cells, talazoparib- and olaparib-resistant cell lines share two hypermethylated sites, *RUVBL1* and *BHLHE40*, and one hypomethylation site in *NEDD4L*. The hypermethylation in *RUVBL1* occurs in a CpG island in the last intron of a transcript variant of *RUVBL1*, at the site of the *RUVBL1-AS* transcript, suggesting a deregulation of *RUVBL1* expression. The hypermethylation in *BHLHE40* covers a CpG island present in the coding region of the final exon. It is also observed in the resistant cell lines FUOV1 and OVCA420, which points to a potential association with olaparib resistance (Figure 6 and Supplemental Table S8). However, a slight increase in methylation in A2780 cells compared with the other cell lines was also found, but it was below the level of significance.

In contrast to the CAOV3 cell lines, significant DMRs were not observed between the parental OVCAR8 and the olaparib-resistant cell line. In the talazoparib-resistant cell line, a promoter hypermethylation of the long transcript variant of *ERCC6* was observed (Supplemental Table S8). *ERCC6* encodes the excision repair cross-complemention group 6, a chromatin remodeling factor and is involved in nucleotide excision repair. However, OVCAR8 cells acquired mutations during the resistance process, which would indicate that there are different resistance mechanisms in the two cell lines. Olaparib- and talazoparib-resistant OVCAR8 cells both displayed mutations in *KPNA2* (c.224A>C, p.N75T), *TUBG1* (c.1239G>A, p.M413I), and *USP1* (c.2147_2165, p.E717Afs*1499), pointing to a potential role of these genes in mediating resistance to PARP inhibitors (Supplemental Table S14[47–49]). Interestingly, the *KPNA2* mutation was already present at a low allelic fraction in the parental cell line (data not shown). Furthermore, a reduction was observed in the allelic fraction of an O-6-methylguanine-DNA methyltransferase (*MGMT*) mutation (c.698C>T, p.P233L) from a nearly homozygous state (AF = 0.88) in the parental cell line to a heterozygous state in the talazoparib- and olaparib-resistant cell lines (AF = 0.55 and 0.33, respectively). To clarify if the p.P233L mutation influences PARPi sensitivity, additional functional experiments are needed. High MGMT expression has been linked to temozolomide resistance in cancer, and several studies reported synergistic effects of temozolomide and PARP inhibitors.[62–64]

Discussion

Stratification of patients for their response to a given chemotherapeutic treatment is important considering the growing number of personalized drugs, which target specific molecular aberrations. This enables the selection of patients, who respond to a given treatment, whereas nonresponders are not unnecessarily exposed to adverse effects and it saves precious time for an effective cure. For determining a useful stratification strategy for PARPi, enormous efforts are undertaken to identify responders.[65] Mutations in one allele of *BRCA1* or *BRCA2* together with loss of the wild-type allele diminishes HR DNA damage repair and renders high-grade ovarian cancers sensitive to PARPi. In addition, recent PARPi clinical studies determine, besides *BRCA* mutation status, efficiency of the HR system as a predictor for therapy response. For example, the homologous recombination deficiency score (eg, NOVA trial for niraparib, NCT01847274) or loss of heterozygosity scores (ARIEL3 trial for rucaparib, NCT01968213) are used. These assays can identify HR-deficient tumors regardless of the underlying mechanisms. On one side, this is an enormous advantage; on the other side, it has been shown that some responders are still not identified. Some patients, who are *BRCA* negative and have a low homologous recombination deficiency score, benefit from a PARPi treatment. Thus, the AllCap assay may close this gap and may function as an additional system to identify responders. Furthermore, other clinical trials are now analyzing the influence of additional mutations on treatment response (eg, for the PARPi niraparib, a trial starts), which will inquire the association of approximately 40 DNA damage response genes to PARPi response (NCT03207347). Besides mutations, epigenetic alterations may result in a homologous repair deficiency. However, a recent phase 2 clinical study did not observe a correlation between *BRCA1* methylation status and olaparib response (NCT00753545).[66] A second recent phase 2 study analyzed *BRCA1* and *RAD51C* methylation status and identified *BRCA1/RAD51C* methylation as a better predictor

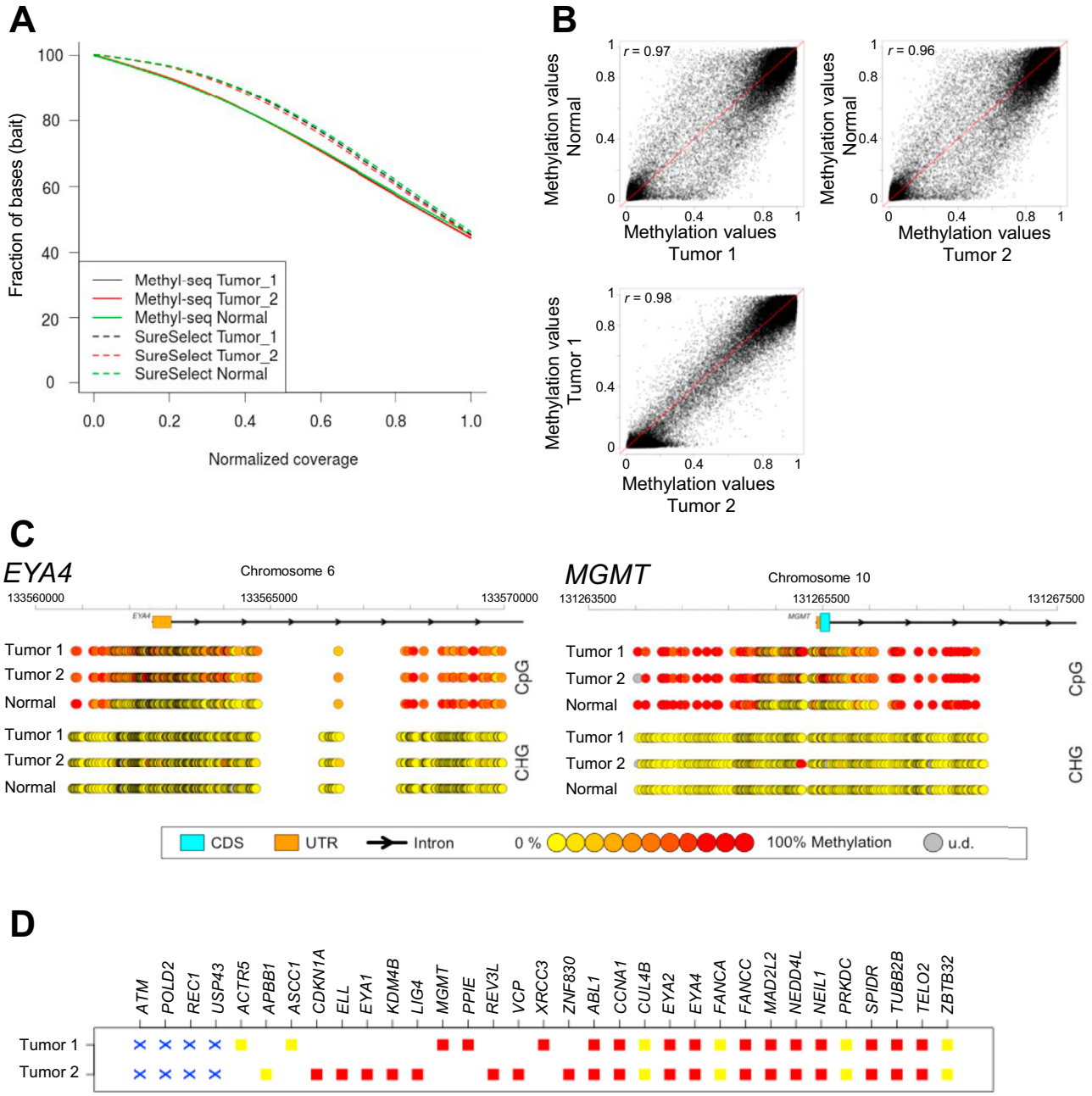

Figure 5 Application of formalin-fixed, paraffin-embedded (FFPE) material with the AllCap assay. **A:** Coverage plot of the three FFPE samples. The fraction of baits (nucleotides) is given on the *y* axis, and the normalized coverage is depicted on the *x* axis. **B:** Scatter plots showing the Pearson's correlation of the methylation levels for each tumor compared with normal (**top panels**) and of the two tumors (**bottom panel**). *r* Value indicates the Pearson correlation coefficient. Only CpGs covered in all samples by ≥10 reads were used for the correlation analysis. Methylation levels of 0 and 1 were excluded from the calculation of the correlation. **C:** Example of two hypermethylated promoter regions, *EYA4* and *MGMT*, in the tumors. Each CpG and CHG is depicted as a circle, and the methylation level is color coded. **D:** Differentially methylated regions (DMRs) and mutations detected in the tumor versus normal comparisons. DMRs were calculated by metilene and filtered for significance ($q < 0.05$). Mutations were calculated by Varbank. Protein altering mutations are displayed. Hypermethylation is depicted in red, and hypomethylation is depicted in yellow. Crosses denote mutations in the corresponding gene. CDS, coding sequence; Seq, sequencing; u.d., undetermined; UTR, untranslated region.

for rucaparib response compared with mutational analysis of HR genes in *BRCA1* wild-type tumors (NCT01891344).[67] Both studies used a single-locus PCR-based approach for testing the methylation level. Having a test on hand like the protocol presented herein will facilitate the analysis of many loci in parallel and help to elucidate the role of DNA methylation in drug response.

To simplify the analysis of DNA methylation in clinical research, the AllCap protocol that allows the parallel analysis of both DNA mutations and methylation was

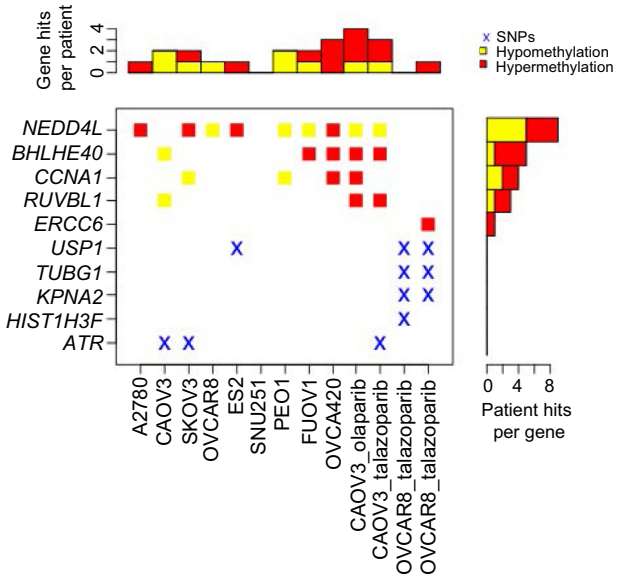

Figure 6 Overview over differentially methylated regions (DMRs) and mutations detected in nine ovary cancer cell lines and four resistant CAOV3 and OVCAR8 cell lines. Shown are genes with DMRs or mutations emerging in the resistant CAOV3 or OVCAR8 cell lines. DMRs were calculated by metilene and filtered for significance ($q < 0.05$). DMRs for the left nine cell lines were calculated in relation to an artificial background over all cell lines, and DMRs for the PARPi resistant cell lines were calculated in relation to their parental sensitive cell line. Mutations were calculated by Varbank, and protein altering mutations are displayed. Hypermethylation is depicted in red, and hypomethylation is depicted in yellow. Crosses denote mutations in the corresponding gene. Cell lines are sorted from sensitive (left A2780) to resistant (right OVCA420). SNP, single-nucleotide polymorphism.

developed. Because a single capture library is used for both, the mutation, and the methylation analysis, the costs for the library preparation kit and the capture library are cut by half. Moreover, hands-on-work time is considerably reduced because most protocol steps take place in parallel.

The protocol was applied on 6, 3, and 1 μg of genomic DNA, and good concordance of the obtained mutations and methylation values was obtained, indicating the validity of the approach.

Because for most clinical applications, 3 μg of input DNA might be too high, the input amount was reduced. Even with 250 ng DNA input, known mutations were reliably detected and correlation of the methylation values between 1 and the 250 ng input was >0.98. However, an increased rate of duplicate reads was received, which has also been described for methyl-sequencing approaches alone with 250 ng, albeit with an increased number of PCR cycles (Agilent application note: Agilent SureSelect^{XT} Methyl-Seq Applications with Low-Input DNA and Smaller Capture Libraries; 5991-7838EN; Santa Clara CA). In addition, because of a diminished bisulfite conversion rate, DNA input amounts <250 ng require further improvements of the protocol. Because a considerable amount of DNA input was lost during the library generation (Supplemental Table S5), additional improvements of the library preparation bear potential to further decrease the amount of DNA input.

Within clinical studies, tissue specimens are routinely used from large tissue banks where samples are stored as FFPE material. Pioneering targeted resequencing studies using FFPE material for next-generation mutational and methylation sequencing already opened an important resource for clinical studies.[44,68–70] Therefore, the AllCap protocol was tested on FFPE material in a proof-of-principle study and sound results were observed. However, in tumor tissue, an uncertain amount of tumor cells and nonneoplastic cells was found, which can make the identification of somatic variants and differential methylation events difficult. Thus, to access the complete performance characteristics of the assay for FFPE material, additional experiments are required. This is in particular also true to access the analytical sensitivity (limit of detection) of the assay.

PARPi resistance is mediated by several genetic lesions. For example, loss of *SLFN11* predicts PARPi resistance in small-cell lung cancer[62] and high *SLFN11* expression corresponds to sensitivity of combinations of PARPi with temozolomide in Ewing sarcoma.[71] Loss of *Trp53bp1*/*Tp53bp1* causes PARPi resistance in a *Brca1*-mutated breast cancer mouse model.[72] Interestingly, mutations were detected in the corresponding human ortholog, *TP53BP1*, in the sensitive SKOV3 cell line (c.1474G>A, p.V429I, AF = 0.74; and c.3573C>A, p.D1191E, AF = 0.16). An increased expression of the phosphoglycolate phosphatase drug efflux transporters, Abcb1a and Abcb1b, mediates resistance to olaparib but not to PARP inhibitors that are not a substrate of phosphoglycolate phosphatase.[73] Such alterations might be due to differential methylations and can thus be detected by the AllCap assay. Moreover, phosphorylation of the mammalian target of rapamycin target ribosomal protein S6 confers PARPi resistance in a *Brca1*-deficient mouse model.[65] Also, PARPi sensitivity has been associated with mutations in several DNA repair genes [eg, *ATM*, *ATR*, *CHEK1*, *CHEK2*, *SEM1* (alias *DSS1*), *FANCA*, *FANCC*, *FANCD2*, *NBN* (alias *NBS1*), *RAD51*, *ATRX* (alias *RAD54*), or *RPA1*].[5,6,8,74] In the pilot experiment, *ATR*, *ATM*, and *EP300* mutations were detected solely in the sensitive cell lines, in line with previously published results.[4,6,8,55,74] Hypermethylation was also found within the basic helix-loop-helix family member E40 (*BHLHE40*; alias *STRA13*, *DEC1*, or *SHARP2*) and the *CCNA1* genes in resistant cell lines. Interestingly, a knockdown of *BHLEH40* decreased the amount of cleaved PARP after treatment with paclitaxel, suggesting that a hypermethylation of the last exon of *BHLHE40* might have an effect on BHLHE40 transcription and on PARP1 level.[75–77] Because we detected a hypermethylation of the *BHLHE40* also in olaparib-resistant cell lines FUOV1 and OVCA420, this might be useful as a biomarker for therapy resistance. However, the potential resistance markers identified herein require an independent validation in a larger cohort and experimental validation.

Taken together, the presented approach will be in particular useful for diagnostic/therapeutic purposes, as has been shown herein using prediction of PARPi sensitivity as an example. Possible implementations of the AllCap assay might be, from a scientific point of view, to identify causes of high homologous recombination deficiency scores and, from a clinical point of view, to identify patients with BRCA-negative and low HR deficiency scores, but who respond to PARPi. A combination of both assay systems may identify more responders. However, additional clinical studies are required to truly develop a clinical assay based on the protocol provided herein. Similarly, for the molecular genetic and epigenetic analyses of imprinting disorders, like Prader-Willi/Angelman syndrome or Beckwith-Wiedemann syndrome, the parallel assessment of mutations or polymorphisms for the discrimination of alleles and differential methylations will be useful. However, other applications include integrated epigenome- and genome-wide association studies to decipher complex diseases and the influence of the genotype on the epigenetic variation.[78,79] Thus, this will open new routes in routine clinical diagnostics, but also basic scientific research.

Acknowledgments

C.G., E.W., R.K., and R.C. performed experiments; A.F., M.L., H.T., and M.H. performed bioinformatic analyses; K.H. designed the capture library and discussed the protocol; J.A. performed next-generation sequencing; A.M.F., R.K., B.T.H., A.M.S., and H.C.R. contributed cell lines and discussions of the data; C.G., R.B., and M.R.S. designed the study and analyzed the data; C.G. and M.R.S. wrote the manuscript.

Supplemental Data

Supplemental material for this article can be found at *https://doi.org/10.1016/j.jmoldx.2018.10.007*.

References

1. Hyman DM, Taylor BS, Baselga J: Implementing genome-driven oncology. Cell 2017, 168:584−599
2. Gao D, Herman JG, Guo M: The clinical value of aberrant epigenetic changes of DNA damage repair genes in human cancer. Oncotarget 2016, 7:37331−37346
3. Nowsheen S, Aziz K, Tran PT, Gorgoulis VG, Yang ES, Georgakilas AG: Epigenetic inactivation of DNA repair in breast cancer. Cancer Lett 2014, 342:213−222
4. Curtin NJ: DNA repair dysregulation from cancer driver to therapeutic target. Nat Rev Cancer 2012, 12:801−817
5. Hosoya N, Miyagawa K: Targeting DNA damage response in cancer therapy. Cancer Sci 2014, 105:370−388
6. Lord CJ, Ashworth A: PARP inhibitors: synthetic lethality in the clinic. Science 2017, 355:1152−1158
7. First PARP inhibitor Ok'd for breast cancer. Cancer Discov 2018, 8: 256−257
8. Lord CJ, Ashworth A: BRCAness revisited. Nat Rev Cancer 2016, 16:110−120
9. Lin KY, Kraus WL: PARP inhibitors for cancer therapy. Cell 2017, 169:183
10. Kamel D, Gray C, Walia JS, Kumar V: PARP inhibitor drugs in the treatment of breast, ovarian, prostate and pancreatic cancers: an update of clinical trials. Curr Drug Targets 2018, 19:21−37
11. Lahtz C, Pfeifer GP: Epigenetic changes of DNA repair genes in cancer. J Mol Cell Biol 2011, 3:51−58
12. Pfeifer GP: Defining driver DNA methylation changes in human cancer. Int J Mol Sci 2018, 19. pii: E1166
13. Llinas-Arias P, Esteller M: Epigenetic inactivation of tumour suppressor coding and non-coding genes in human cancer: an update. Open Biol 2017, 7:170152
14. Shen H, Laird PW: Interplay between the cancer genome and epigenome. Cell 2013, 153:38−55
15. Frampton GM, Fichtenholtz A, Otto GA, Wang K, Downing SR, He J, et al: Development and validation of a clinical cancer genomic profiling test based on massively parallel DNA sequencing. Nat Biotechnol 2013, 31:1023−1031
16. Zehir A, Benayed R, Shah RH, Syed A, Middha S, Kim HR, et al: Mutational landscape of metastatic cancer revealed from prospective clinical sequencing of 10,000 patients. Nat Med 2017, 23:703−713
17. Wang Y, Chen PM, Liu RB: Advance in plasma SEPT9 gene methylation assay for colorectal cancer early detection. World J Gastrointest Oncol 2018, 10:15−22
18. Lamb YN, Dhillon S: Epi proColon((R)) 2.0 CE: a blood-based screening test for colorectal cancer. Mol Diagn Ther 2017, 21: 225−232
19. Moran S, Martinez-Cardus A, Boussios S, Esteller M: Precision medicine based on epigenomics: the paradigm of carcinoma of unknown primary. Nat Rev Clin Oncol 2017, 14:682−694
20. Mijnes J, Veeck J, Gaisa NT, Burghardt E, de Ruijter TC, Gostek S, Dahl E, Pfister D, Schmid SC, Knuchel R, Rose M: Promoter methylation of DNA damage repair (DDR) genes in human tumor entities: RBBP8/CtIP is almost exclusively methylated in bladder cancer. Clin Epigenet 2018, 10:15
21. Leygo C, Williams M, Jin HC, Chan MWY, Chu WK, Grusch M, Cheng YY: DNA methylation as a noninvasive epigenetic biomarker for the detection of cancer. Dis Markers 2017, 2017:3726595
22. Koch A, Joosten SC, Feng Z, de Ruijter TC, Draht MX, Melotte V, Smits KM, Veeck J, Herman JG, Neste LV, Criekinge WV, De Meyer T, Engeland MV: Analysis of DNA methylation in cancer: location revisited. Nat Rev Clin Oncol 2018, 15:459−466
23. BLUEPRINT consortium: Quantitative comparison of DNA methylation assays for biomarker development and clinical applications. Nat Biotechnol 2016, 34:726−737
24. Stordal B, Timms K, Farrelly A, Gallagher D, Busschots S, Renaud M, Thery J, Williams D, Potter J, Tran T, Korpanty G, Cremona M, Carey M, Li J, Li Y, Aslan O, O'Leary JJ, Mills GB, Hennessy BT: BRCA1/2 mutation analysis in 41 ovarian cell lines reveals only one functionally deleterious BRCA1 mutation. Mol Oncol 2013, 7:567−579
25. Barretina J, Caponigro G, Stransky N, Venkatesan K, Margolin AA, Kim S, et al: The Cancer Cell Line Encyclopedia enables predictive modelling of anticancer drug sensitivity. Nature 2012, 483:603−607
26. Karolchik D, Hinrichs AS, Furey TS, Roskin KM, Sugnet CW, Haussler D, Kent WJ: The UCSC Table Browser data retrieval tool. Nucleic Acids Res 2004, 32:D493−D496
27. McLaren W, Gil L, Hunt SE, Riat HS, Ritchie GR, Thormann A, Flicek P, Cunningham F: The Ensembl variant effect predictor. Genome Biol 2016, 17:122
28. Landrum MJ, Lee JM, Benson M, Brown G, Chao C, Chitipiralla S, Gu B, Hart J, Hoffman D, Hoover J, Jang W, Katz K, Ovetsky M, Riley G, Sethi A, Tully R, Villamarin-Salomon R, Rubinstein W, Maglott DR: ClinVar: public archive of interpretations of clinically relevant variants. Nucleic Acids Res 2016, 44:D862−D868

29. Xi Y, Li W: BSMAP: whole genome bisulfite sequence MAPping program. BMC Bioinform 2009, 10:232
30. Li H, Handsaker B, Wysoker A, Fennell T, Ruan J, Homer N, Marth G, Abecasis G, Durbin R; 1000 Genome Project Data Processing Subgroup: The sequence alignment/map format and SAMtools. Bioinformatics 2009, 25:2078−2079
31. Quinlan AR, Hall IM: BEDTools: a flexible suite of utilities for comparing genomic features. Bioinformatics 2010, 26:841−842
32. Kent WJ, Zweig AS, Barber G, Hinrichs AS, Karolchik D: BigWig and BigBed: enabling browsing of large distributed datasets. Bioinformatics 2010, 26:2204−2207
33. Thorvaldsdottir H, Robinson JT, Mesirov JP: Integrative Genomics Viewer (IGV): high-performance genomics data visualization and exploration. Brief Bioinform 2013, 14:178−192
34. Robinson JT, Thorvaldsdottir H, Winckler W, Guttman M, Lander ES, Getz G, Mesirov JP: Integrative genomics viewer. Nat Biotechnol 2011, 29:24−26
35. Juhling F, Kretzmer H, Bernhart SH, Otto C, Stadler PF, Hoffmann S: metilene: fast and sensitive calling of differentially methylated regions from bisulfite sequencing data. Genome Res 2016, 26:256−262
36. Aryee MJ, Jaffe AE, Corrada-Bravo H, Ladd-Acosta C, Feinberg AP, Hansen KD, Irizarry RA: Minfi: a flexible and comprehensive Bioconductor package for the analysis of Infinium DNA methylation microarrays. Bioinformatics 2014, 30:1363−1369
37. Lee EJ, Pei L, Srivastava G, Joshi T, Kushwaha G, Choi JH, Robertson KD, Wang X, Colbourne JK, Zhang L, Schroth GP, Xu D, Zhang K, Shi H: Targeted bisulfite sequencing by solution hybrid selection and massively parallel sequencing. Nucleic Acids Res 2011, 39:e127
38. Fabregat A, Jupe S, Matthews L, Sidiropoulos K, Gillespie M, Garapati P, Haw R, Jassal B, Korninger F, May B, Milacic M, Roca CD, Rothfels K, Sevilla C, Shamovsky V, Shorser S, Varusai T, Viteri G, Weiser J, Wu G, Stein L, Hermjakob H, D'Eustachio P: The Reactome Pathway Knowledgebase. Nucleic Acids Res 2018, 46:D649−D655
39. Kanehisa M, Goto S: KEGG: Kyoto Encyclopedia of Genes and Genomes. Nucleic Acids Res 2000, 28:27−30
40. Kanehisa M, Sato Y, Kawashima M, Furumichi M, Tanabe M: KEGG as a reference resource for gene and protein annotation. Nucleic Acids Res 2016, 44:D457−D462
41. Kanehisa M, Furumichi M, Tanabe M, Sato Y, Morishima K: KEGG: new perspectives on genomes, pathways, diseases and drugs. Nucleic Acids Res 2017, 45:D353−D361
42. Milanowska K, Krwawicz J, Papaj G, Kosinski J, Poleszak K, Lesiak J, Osinska E, Rother K, Bujnicki JM: REPAIRtoire: a database of DNA repair pathways. Nucleic Acids Res 2011, 39:D788−D792
43. Szklarczyk D, Morris JH, Cook H, Kuhn M, Wyder S, Simonovic M, Santos A, Doncheva NT, Roth A, Bork P, Jensen LJ, von Mering C: The STRING database in 2017: quality-controlled protein-protein association networks, made broadly accessible. Nucleic Acids Res 2017, 45:D362−D368
44. Kerick M, Isau M, Timmermann B, Sultmann H, Herwig R, Krobitsch S, Schaefer G, Verdorfer I, Bartsch G, Klocker H, Lehrach H, Schweiger MR: Targeted high throughput sequencing in clinical cancer settings: formaldehyde fixed-paraffin embedded (FFPE) tumor tissues, input amount and tumor heterogeneity. BMC Med Genom 2011, 4:68
45. Li Q, Suzuki M, Wendt J, Patterson N, Eichten SR, Hermanson PJ, Green D, Jeddeloh J, Richmond T, Rosenbaum H, Burgess D, Springer NM, Greally JM: Post-conversion targeted capture of modified cytosines in mammalian and plant genomes. Nucleic Acids Res 2015, 43:e81
46. Yang W, Soares J, Greninger P, Edelman EJ, Lightfoot H, Forbes S, Bindal N, Beare D, Smith JA, Thompson IR, Ramaswamy S, Futreal PA, Haber DA, Stratton MR, Benes C, McDermott U, Garnett MJ: Genomics of Drug Sensitivity in Cancer (GDSC): a resource for therapeutic biomarker discovery in cancer cells. Nucleic Acids Res 2013, 41:D955−D961
47. Adzhubei I, Jordan DM, Sunyaev SR: Predicting functional effect of human missense mutations using PolyPhen-2. Curr Protoc Hum Genet 2013. Chapter 7:Unit 7.20
48. Kumar P, Henikoff S, Ng PC: Predicting the effects of coding non-synonymous variants on protein function using the SIFT algorithm. Nat Protoc 2009, 4:1073−1081
49. Petrovski S, Wang Q, Heinzen EL, Allen AS, Goldstein DB: Genic intolerance to functional variation and the interpretation of personal genomes. PLoS Genet 2013, 9:e1003709
50. Kim H, George E, Ragland R, Rafial S, Zhang R, Krepler C, Morgan M, Herlyn M, Brown E, Simpkins F: Targeting the ATR/CHK1 axis with PARP inhibition results in tumor regression in BRCA-mutant ovarian cancer models. Clin Cancer Res 2017, 23:3097−3108
51. Murai J, Feng Y, Yu GK, Ru Y, Tang SW, Shen Y, Pommier Y: Resistance to PARP inhibitors by SLFN11 inactivation can be overcome by ATR inhibition. Oncotarget 2016, 7:76534−76550
52. Yazinski SA, Comaills V, Buisson R, Genois MM, Nguyen HD, Ho CK, Todorova Kwan T, Morris R, Lauffer S, Nussenzweig A, Ramaswamy S, Benes CH, Haber DA, Maheswaran S, Birrer MJ, Zou L: ATR inhibition disrupts rewired homologous recombination and fork protection pathways in PARP inhibitor-resistant BRCA-deficient cancer cells. Genes Dev 2017, 31:318−332
53. Schmitt A, Knittel G, Welcker D, Yang TP, George J, Nowak M, Leeser U, Buttner R, Perner S, Peifer M, Reinhardt HC: ATM deficiency is associated with sensitivity to PARP1- and ATR inhibitors in lung adenocarcinoma. Cancer Res 2017, 77:3040−3056
54. Knittel G, Rehkamper T, Korovkina D, Liedgens P, Fritz C, Torgovnick A, Al-Baldawi Y, Al-Maarri M, Cun Y, Fedorchenko O, Riabinska A, Beleggia F, Nguyen PH, Wunderlich FT, Ortmann M, Montesinos-Rongen M, Tausch E, Stilgenbauer S, P Frenzel L, Herling M, Herling C, Bahlo J, Hallek M, Peifer M, Buettner R, Persigehl T, Reinhardt HC: Two mouse models reveal an actionable PARP1 dependence in aggressive chronic lymphocytic leukemia. Nat Commun 2017, 8:153
55. Carter RJ, Parsons JL: Base excision repair, a pathway regulated by posttranslational modifications. Mol Cell Biol 2016, 36:1426−1437
56. Bai P: Biology of poly(ADP-ribose) polymerases: the factotums of cell maintenance. Mol Cell 2015, 58:947−958
57. Hassa PO, Buerki C, Lombardi C, Imhof R, Hottiger MO: Transcriptional coactivation of nuclear factor-kappaB-dependent gene expression by p300 is regulated by poly(ADP)-ribose polymerase-1. J Biol Chem 2003, 278:45145−45153
58. Faraoni I, Aloisio F, De Gabrieli A, Consalvo MI, Lavorgna S, Voso MT, Lo-Coco F, Graziani G: The poly(ADP-ribose) polymerase inhibitor olaparib induces up-regulation of death receptors in primary acute myeloid leukemia blasts by NF-kappaB activation. Cancer Lett 2018, 423:127−138
59. Robaszkiewicz A, Wisnik E, Regdon Z, Chmielewska K, Virag L: PARP1 facilitates EP300 recruitment to the promoters of the subset of RBL2-dependent genes. Biochim Biophys Acta 2018, 1861:41−53
60. Wang C, Jette N, Moussienko D, Bebb DG, Lees-Miller SP: ATM-deficient colorectal cancer cells are sensitive to the PARP inhibitor olaparib. Transl Oncol 2017, 10:190−196
61. Wilson IM, Vucic EA, Enfield KS, Thu KL, Zhang YA, Chari R, Lockwood WW, Radulovich N, Starczynowski DT, Banath JP, Zhang M, Pusic A, Fuller M, Lonergan KM, Rowbotham D, Yee J, English JC, Buys TP, Selamat SA, Laird-Offringa IA, Liu P, Anderson M, You M, Tsao MS, Brown CJ, Bennewith KL, MacAulay CE, Karsan A, Gazdar AF, Lam S, Lam WL: EYA4 is inactivated biallelically at a high frequency in sporadic lung cancer and is associated with familial lung cancer risk. Oncogene 2014, 33:4464−4473
62. Lok BH, Gardner EE, Schneeberger VE, Ni A, Desmeules P, Rekhtman N, de Stanchina E, Teicher BA, Riaz N, Powell SN,

Poirier JT, Rudin CM: PARP inhibitor activity correlates with SLFN11 expression and demonstrates synergy with temozolomide in small cell lung cancer. Clin Cancer Res 2017, 23:523−535

63. Tentori L, Ricci-Vitiani L, Muzi A, Ciccarone F, Pelacchi F, Calabrese R, Runci D, Pallini R, Caiafa P, Graziani G: Pharmacological inhibition of poly(ADP-ribose) polymerase-1 modulates resistance of human glioblastoma stem cells to temozolomide. BMC Cancer 2014, 14:151
64. Horton TM, Jenkins G, Pati D, Zhang L, Dolan ME, Ribes-Zamora A, Bertuch AA, Blaney SM, Delaney SL, Hegde M, Berg SL: Poly(ADP-ribose) polymerase inhibitor ABT-888 potentiates the cytotoxic activity of temozolomide in leukemia cells: influence of mismatch repair status and O6-methylguanine-DNA methyltransferase activity. Mol Cancer Ther 2009, 8: 2232−2242
65. Sun CK, Zhang F, Xiang T, Chen Q, Pandita TK, Huang Y, Hu MC, Yang Q: Phosphorylation of ribosomal protein S6 confers PARP inhibitor resistance in BRCA1-deficient cancers. Oncotarget 2014, 5: 3375−3385
66. Lheureux S, Lai Z, Dougherty BA, Runswick S, Hodgson DR, Timms KM, Lanchbury JS, Kaye S, Gourley C, Bowtell D, Kohn EC, Scott C, Matulonis U, Panzarella T, Karakasis K, Burnier JV, Gilks CB, O'Connor MJ, Robertson JD, Ledermann J, Barrett JC, Ho TW, Oza AM: Long-term responders on olaparib maintenance in high-grade serous ovarian cancer: clinical and molecular characterization. Clin Cancer Res 2017, 23:4086−4094
67. Swisher EM, Lin KK, Oza AM, Scott CL, Giordano H, Sun J, Konecny GE, Coleman RL, Tinker AV, O'Malley DM, Kristeleit RS, Ma L, Bell-McGuinn KM, Brenton JD, Cragun JM, Oaknin A, Ray-Coquard I, Harrell MI, Mann E, Kaufmann SH, Floquet A, Leary A, Harding TC, Goble S, Maloney L, Isaacson J, Allen AR, Rolfe L, Yelensky R, Raponi M, McNeish IA: Rucaparib in relapsed, platinum-sensitive high-grade ovarian carcinoma (ARIEL2 Part 1): an international, multicentre, open-label, phase 2 trial. Lancet Oncol 2017, 18:75−87
68. Schweiger MR, Kerick M, Timmermann B, Albrecht MW, Borodina T, Parkhomchuk D, Zatloukal K, Lehrach H: Genome-wide massively parallel sequencing of formaldehyde fixed-paraffin embedded (FFPE) tumor tissues for copy-number- and mutation-analysis. PLoS One 2009, 4:e5548
69. Wood HM, Belvedere O, Conway C, Daly C, Chalkley R, Bickerdike M, McKinley C, Egan P, Ross L, Hayward B, Morgan J, Davidson L, MacLennan K, Ong TK, Papagiannopoulos K, Cook I, Adams DJ, Taylor GR, Rabbitts P: Using next-generation sequencing for high resolution multiplex analysis of copy number variation from nanogram quantities of DNA from formalin-fixed paraffin-embedded specimens. Nucleic Acids Res 2010, 38:e151
70. Gu H, Bock C, Mikkelsen TS, Jager N, Smith ZD, Tomazou E, Gnirke A, Lander ES, Meissner A: Genome-scale DNA methylation mapping of clinical samples at single-nucleotide resolution. Nat Methods 2010, 7:133−136
71. Tang SW, Bilke S, Cao L, Murai J, Sousa FG, Yamade M, Rajapakse V, Varma S, Helman LJ, Khan J, Meltzer PS, Pommier Y: SLFN11 is a transcriptional target of EWS-FLI1 and a determinant of drug response in Ewing sarcoma. Clin Cancer Res 2015, 21:4184−4193
72. Jaspers JE, Kersbergen A, Boon U, Sol W, van Deemter L, Zander SA, Drost R, Wientjens E, Ji J, Aly A, Doroshow JH, Cranston A, Martin NM, Lau A, O'Connor MJ, Ganesan S, Borst P, Jonkers J, Rottenberg S: Loss of 53BP1 causes PARP inhibitor resistance in Brca1-mutated mouse mammary tumors. Cancer Discov 2013, 3:68−81
73. Henneman L, van Miltenburg MH, Michalak EM, Braumuller TM, Jaspers JE, Drenth AP, de Korte-Grimmerink R, Gogola E, Szuhai K, Schlicker A, Bin Ali R, Pritchard C, Huijbers IJ, Berns A, Rottenberg S, Jonkers J: Selective resistance to the PARP inhibitor olaparib in a mouse model for BRCA1-deficient metaplastic breast cancer. Proc Natl Acad Sci U S A 2015, 112:8409−8414
74. Dietlein F, Thelen L, Reinhardt HC: Cancer-specific defects in DNA repair pathways as targets for personalized therapeutic approaches. Trends Genet 2014, 30:326−339
75. Wu Y, Sato F, Bhawal UK, Kawamoto T, Fujimoto K, Noshiro M, Morohashi S, Kato Y, Kijima H: Basic helix-loop-helix transcription factors DEC1 and DEC2 regulate the paclitaxel-induced apoptotic pathway of MCF-7 human breast cancer cells. Int J Mol Med 2011, 27:491−495
76. Liu Q, Wu Y, Yoshizawa T, Yan X, Morohashi S, Seino H, Kato Y, Kijima H: Basic helix-loop-helix transcription factor DEC2 functions as an anti-apoptotic factor during paclitaxel-induced apoptosis in human prostate cancer cells. Int J Mol Med 2016, 38:1727−1733
77. Seino H, Wu Y, Morohashi S, Kawamoto T, Fujimoto K, Kato Y, Takai Y, Kijima H: Basic helix-loop-helix transcription factor DEC1 regulates the cisplatin-induced apoptotic pathway of human esophageal cancer cells. Biomed Res 2015, 36:89−96
78. Rakyan VK, Down TA, Balding DJ, Beck S: Epigenome-wide association studies for common human diseases. Nat Rev Genet 2011, 12:529−541
79. Wu Y, Zeng J, Zhang F, Zhu Z, Qi T, Zheng Z, Lloyd-Jones LR, Marioni RE, Martin NG, Montgomery GW, Deary IJ, Wray NR, Visscher PM, McRae AF, Yang J: Integrative analysis of omics summary data reveals putative mechanisms underlying complex traits. Nat Commun 2018, 9:918